

# Ensemble perspective for understanding temporal credit assignment

Wenxuan Zou,<sup>\*</sup> Chan Li,<sup>\*</sup> and Haiping Huang<sup>†</sup>

*PMI Lab, School of Physics, Sun Yat-sen University, Guangzhou 510275, People's Republic of China*

(Dated: December 23, 2024)

Recurrent neural networks are widely used for modeling spatio-temporal sequences in both nature language processing and neural population dynamics. However, understanding the temporal credit assignment is hard. Here, we propose that each individual connection in the recurrent computation is modeled by a spike and slab distribution, rather than a precise weight value. We then derive the mean-field algorithm to train the network at the ensemble level. The method is then applied to classify handwritten digits when pixels are read in sequence, and to the multisensory integration task that is a fundamental cognitive function of animals. Our model reveals important connections that determine the overall performance of the network. The model also shows how spatio-temporal information is processed through the hyperparameters of the distribution, and moreover reveals distinct types of emergent neural selectivity. It is thus promising to study the temporal credit assignment in recurrent neural networks from the ensemble perspective.

## I. INTRODUCTION

Recurrence is ubiquitous in the brain. Neural networks with reciprocally connected recurrent units are called recurrent neural networks (RNN). Because of feedback supports provided by these recurrent units, this type of neural networks is able to maintain information about sensory inputs across temporal domains, and thus plays an important role in processing time-dependent sequences, thereby widely used as a basic computational block in nature language processing [1–6] and even modeling brain dynamics in various kinds of neural circuits [7–10].

Training RNNs is in general very challenging, because of the intrinsic difficulty in capturing long-term dependence of the sequences. Advanced architectures commonly introduce gating mechanisms, e.g., the long short-term memory network (LSTM) with multiplicative gates controlling the information flow across time steps [1], or a simplified variant—gated recurrent unit network (GRU) [6]. All these recurrent neural networks are commonly trained by backpropagation through time (BPTT) [11, 12], which sums up all gradient (of the loss function) contributions over all time steps of a trial, to update the recurrent network parameters. The training is terminated until a specific network yields a satisfied generalization accuracy on unseen trials (time-dependent sequences). This specific network is clearly a point-estimate of the candidate architecture realizing the desired computational task. A recent study of learning (spatial) credit assignment suggests that an ensemble of candidate networks, instead of the traditional point-estimate, can be successfully learned at a cheap computational cost, and particularly yields statistical properties of the trained network [13]. The ensemble training is achieved by only defining a spike and slab (SaS) probability distribution for each network connection, which offers an opportunity to look at the relevance of each connection to the macroscopic behavioral output of the network. Therefore, we expect that a similar perspective applies to the RNNs, and an ensemble of candidate networks can also emerge during training of the SaS probability distributions for RNNs.

Weight uncertainty is a key concept in studying neural circuits [14]. The stochastic nature of computation appears not only in the earlier sensory layers but also in deep layers of internal dynamics. Revealing the underlying mechanism about how the uncertainty is combined with the recurrent dynamics becomes essential to interpret the behavior of RNNs. In particular, addressing how a RNN learns a probability distribution over weights could provide potential insights towards understanding of learning in the brain. There may exist a long-term dependence in the recurrent dynamics, and both directions of one connection may carry distinct information in a spatio-temporal domain. How a training at the ensemble level combines these intrinsic properties of RNNs thus becomes intriguing. In this work, we derive a mean-field method to train RNNs, considering a weight distribution for each direction of connection. We then test our method on both MNIST dataset in a sequence-learning setting [15] and multi-sensory integration tasks [16–18]. The multi-sensory integration tasks are relevant to computational modeling of cognitive experiments of rodents and primates.

By analyzing the distribution of the model parameters, and its relationship with the computational task, and

---

<sup>\*</sup>W.Z. and C.L. contributed equally to this work.

<sup>†</sup>Electronic address: huanghp7@mail.sysu.edu.cn

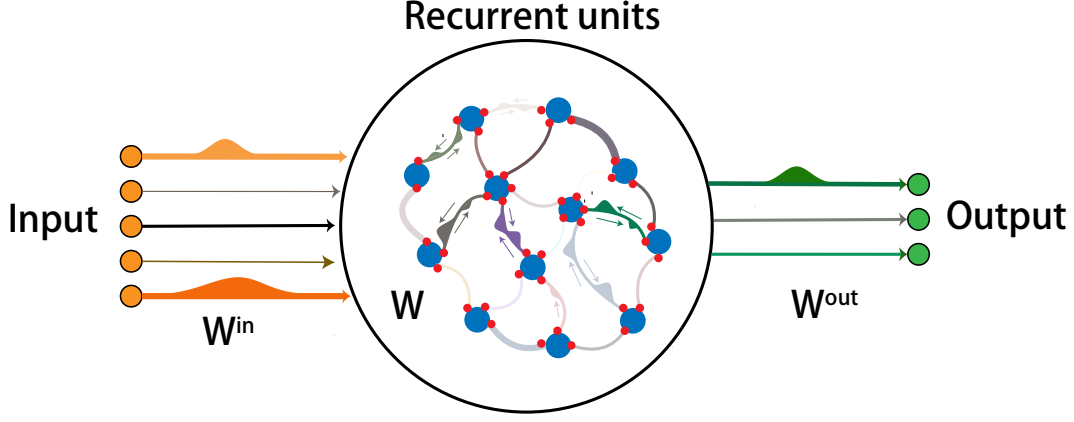


FIG. 1: Illustration of a RNN learning the temporal credit assignment. Each connection is described by the spike and slab distribution; the spike indicates the corresponding synaptic weight absent for a task, while the slab represents a Gaussian distribution responsible for the weight uncertainty. The Gaussian slab is displayed in the plot, and the arrow in the reservoir shows different directions of information flow. Different sizes of connection show how probable these connections should be present during recurrent computation.

moreover the selectivity of each recurrent unit, we are able to provide mechanistic understanding about the recurrent dynamics in both engineering applications and computational neuroscience modeling. Our method learns the statistics of the RNN ensemble, producing a dynamic architecture that adapts to temporally varying inputs, which thereby goes beyond traditional training protocols focusing on a stationary network topology. The hyperparameters governing the weight distribution reveal which credit assignments are critical to the network behavior, which further explains distinct functions of each computational layer and the emergent neural selectivity. Therefore, our ensemble theory can be used as a promising tool to explore internal dynamics of widely used RNNs.

## II. MODEL AND ENSEMBLE TRAINING

In this study, we consider a recurrent neural network processing a time-dependent input  $\mathbf{x}(t)$  of time length  $T$ . The input signal is sent to the recurrent reservoir via the input weight matrix  $\mathbf{W}^{\text{in}}$ . The number of input units are determined by design details of the task, and  $w_{ij}^{\text{in}}$  denotes the weight value for the connection from input unit  $j$  to recurrent node  $i$ . The neural responses of recurrent units are represented by an activity vector  $\mathbf{r}(t)$  at time step  $t$ . We define  $w_{ij}$  as the connection from node  $j$  to node  $i$  in the reservoir. In general,  $w_{ij} \neq w_{ji}$ , indicating different weights for different directions of information flow. In addition, we do not preclude the self-interaction  $w_{ii}$ , which can be used to maintain the representation encoded in the history of the internal dynamics [19]. The specific statistics of this self-interaction can be determined by the learning shown below. The internal activity  $\mathbf{r}(t)$  is read out through the output matrix  $\mathbf{W}^{\text{out}}$  in the form of the time-dependent output  $\mathbf{y}(t)$ .

We first define  $h_i(t)$  as the time-dependent synaptic current of neuron  $i$ . The dynamics of the recurrent network can thus be summarized as follows,

$$h_i(t+1) = (1 - \alpha)h_i(t) + \alpha u_i(t+1) + \sqrt{2\alpha\sigma^2}n_i, \quad (1a)$$

$$u_i(t+1) = \sum_{j=1}^N w_{ij} r_j(t) + \sum_{j=1}^N w_{ij}^{\text{in}} x_j(t+1), \quad (1b)$$

$$r_i(t) = \phi(h_i(t)), \quad (1c)$$

$$z_k(t) = \sum_{i=1}^N w_{ki}^{\text{out}} r_i(t), \quad (1d)$$

$$y_k(t) = f(z_k(t)), \quad (1e)$$

where  $u(\cdot)$  is the pre-activation function,  $\phi(\cdot)$  denotes the nonlinear transfer function, for which we use the rectified linear unit (ReLU) function for all tasks.  $\alpha = \frac{\Delta t}{\tau}$ , where  $\Delta t$  is a small time interval (e.g., emerging from discretization of a continuous dynamics [20]), and  $\tau$  denotes the time constant of the dynamics.  $n_i \sim \mathcal{N}(0, 1)$  indicates a normally

distributed random number with zero mean and unit variance, sampled independently at every time step, and  $\sigma$  controls the strength of the recurrent noise intrinsic to the network. This intrinsic noise is present in modeling cognitive tasks, but absent for engineering applications. Considering a Gaussian white noise and a baseline ( $\mathbf{x}_0$ ), we write the input vector  $\mathbf{x}(t)$  as

$$\mathbf{x}(t) = \mathbf{x}_0 + \mathbf{x}_t^{\text{task}} + \sqrt{2\sigma_{\text{in}}^2/\alpha}\boldsymbol{\xi}, \quad (2)$$

where the input has been written in a discrete time form,  $\mathbf{x}_t^{\text{task}}$  denotes the sequence of the task, and  $\xi_i \sim \mathcal{N}(0, 1)$ , which is independently sampled at each time step. The noise term is also called the external sensory noise of strength  $\sigma_{\text{in}}$ , commonly observed in brain circuits [21, 22], but is absent in engineering applications.

For a MNIST classification task,  $f(\cdot)$  is chosen to be the softmax function, specifying the probability over all the classes at the last time step  $T$ , i.e.,  $y_k(T) = \frac{e^{z_k(T)}}{\sum_j e^{z_j(T)}}$ . We define  $\hat{y}_k$  as the target label (one-hot form), and use the cross entropy  $\mathcal{L} = -\sum_i \hat{y}_i \ln y_i(T)$  as the loss function to be minimized. For a multisensory integration task,  $f(\cdot)$  is an identity function, and the mean squared-error is chosen to be the objective function.

To search for the optimal random network ensemble for time-dependent tasks in recurrent neural networks, we model the statistics of the weight matrices by the SaS probability distribution [13] as follows,

$$P(w_{ij}^{\text{in}}) = \pi_{ij}^{\text{in}}\delta(w_{ij}^{\text{in}}) + (1 - \pi_{ij}^{\text{in}})\mathcal{N}(w_{ij}^{\text{in}}|m_{ij}^{\text{in}}, \Xi_{ij}^{\text{in}}), \quad (3a)$$

$$P(w_{ij}) = \pi_{ij}\delta(w_{ij}) + (1 - \pi_{ij})\mathcal{N}(w_{ij}|m_{ij}, \Xi_{ij}), \quad (3b)$$

$$P(w_{ki}^{\text{out}}) = \pi_{ki}^{\text{out}}\delta(w_{ki}^{\text{out}}) + (1 - \pi_{ki}^{\text{out}})\mathcal{N}(w_{ki}^{\text{out}}|m_{ki}^{\text{out}}, \Xi_{ki}^{\text{out}}). \quad (3c)$$

The spike mass at  $\delta(\cdot)$  is related to the network compression, indicating the necessary weight resources required for a specific task. The continuous slab,  $\mathcal{N}(w_{ij}|m_{ij}, \Xi_{ij})$ , denotes the Gaussian distribution with mean  $m_{ij}$  and variance  $\Xi_{ij}$ , characterizing the weight uncertainty when the corresponding connection can not be absent (see Fig. 1).

Next, we derive the learning equations about how the SaS parameters are updated, based on mean-field approximation. More precisely, we consider the average over the statistics of the network ensemble during training. Notice that, the first and second moments of the weight  $w_{ij}$  for three sets of weights can be written in a common form as  $\mu_{ij} = (1 - \pi_{ij})m_{ij}$  and  $\varrho_{ij} = (1 - \pi_{ij})(m_{ij}^2 + \Xi_{ij})$ . Given a large fan-in, the pre-activation  $u_i(t)$  and the output  $z_i(t)$  can be re-parametrized by using standard Gaussian random variables, i.e., it is reasonable to assume that they are subject to  $\mathcal{N}(u_i(t)|G_i^{\text{in}}(t) + G_i^{\text{rec}}(t-1), \sqrt{(\Delta_i^{\text{in}}(t))^2 + (\Delta_i^{\text{rec}}(t-1))^2})$  and  $\mathcal{N}(z_i(t)|G_i^{\text{out}}(t), \Delta_i^{\text{out}}(t))$ , respectively, according to the central-limit-theorem. Note that when the number of fan-in to a recurrent unit is small, the central-limit-theorem may break. In this situation, we take the deterministic limit. Therefore, the mean-field dynamics of the model becomes

$$h_i(t+1) = (1 - \alpha)h_i(t) + \alpha u_i(t+1) + \sqrt{2\alpha\sigma^2}n_i, \quad (4a)$$

$$u_i(t+1) = G_i^{\text{rec}}(t) + G_i^{\text{in}}(t+1) + \epsilon_i^{\text{u}}(t+1)\sqrt{(\Delta_i^{\text{in}}(t+1))^2 + (\Delta_i^{\text{rec}}(t))^2}, \quad (4b)$$

$$r_i(t) = \phi(h_i(t)), \quad (4c)$$

$$z_k(t) = G_k^{\text{out}}(t) + \epsilon_k^{\text{out}}(t)\Delta_k^{\text{out}}(t), \quad (4d)$$

$$y_k(t) = f(z_k(t)), \quad (4e)$$

where

$$G_i^{\text{in}}(t+1) = \sum_j \mu_{ij}^{\text{in}}x_j(t+1), \quad (5a)$$

$$G_i^{\text{rec}}(t+1) = \sum_j \mu_{ij}r_j(t+1), \quad (5b)$$

$$G_k^{\text{out}}(t+1) = \sum_i \mu_{ki}^{\text{out}}r_i(t+1), \quad (5c)$$

$$(\Delta_i^{\text{in}}(t+1))^2 = \sum_j (\varrho_{ij}^{\text{in}} - (\mu_{ij}^{\text{in}})^2)(x_j(t+1))^2, \quad (5d)$$

$$(\Delta_i^{\text{rec}}(t+1))^2 = \sum_j (\varrho_{ij} - (\mu_{ij})^2)(r_j(t+1))^2, \quad (5e)$$

$$(\Delta_k^{\text{out}}(t+1))^2 = \sum_i (\varrho_{ki}^{\text{out}} - (\mu_{ki}^{\text{out}})^2)(r_i(t+1))^2. \quad (5f)$$

Note that  $\{\epsilon^u(t)\}$  and  $\{\epsilon^{\text{out}}(t)\}$  are both independent random variables sampled from the standard Gaussian distribution with zero mean and unit variance, which are quenched for every single training mini-epoch and also time-step dependent, maintaining the same sequence of values in both feedforward and backward computations.

Updating the network parameters  $(\theta_{ik}^{\text{in}}, \theta_{ik}, \theta_{ki}^{\text{out}})$  can be achieved by the gradient descent on the objective function  $\mathcal{L}$ . First of all, we update  $\theta_{ki}^{\text{out}} \equiv (m_{ki}^{\text{out}}, \pi_{ki}^{\text{out}}, \Xi_{ki}^{\text{out}})$ .

$$\frac{\partial \mathcal{L}}{\partial m_{ki}^{\text{out}}} = \sum_{t=0}^T \frac{\partial \mathcal{L}}{\partial z_k(t)} \frac{\partial z_k(t)}{\partial m_{ki}^{\text{out}}}, \quad (6a)$$

$$\frac{\partial \mathcal{L}}{\partial \pi_{ki}^{\text{out}}} = \sum_{t=0}^T \frac{\partial \mathcal{L}}{\partial z_k(t)} \frac{\partial z_k(t)}{\partial \pi_{ki}^{\text{out}}}, \quad (6b)$$

$$\frac{\partial \mathcal{L}}{\partial \Xi_{ki}^{\text{out}}} = \sum_{t=0}^T \frac{\partial \mathcal{L}}{\partial z_k(t)} \frac{\partial z_k(t)}{\partial \Xi_{ki}^{\text{out}}}, \quad (6c)$$

where  $\frac{\partial \mathcal{L}}{\partial z_k(t)}$  is related to the form of the loss function. For categorization tasks,  $f(\cdot)$  is chosen to be the softmax function, and we use the cross entropy as our objective function, for which  $\frac{\partial \mathcal{L}}{\partial z_k(t)} = (y_k(T) - \hat{y}_k)\delta_{t,T}$ . It is worth noticing that for multi-sensory integration tasks, this derivative does not vanish at intermediate time steps and become thus time-dependent. The other term  $\frac{\partial z_k(t)}{\partial \theta_{ki}^{\text{out}}}$  can be directly computed, showing how sensitive the network activity is read out under the change of the SaS parameters in the output layer:

$$\frac{\partial z_k(t)}{\partial m_{ki}^{\text{out}}} = (1 - \pi_{ki}^{\text{out}})r_i(t) + \frac{\epsilon_k^{\text{out}}(t)(\mu_{ki}^{\text{out}} \pi_{ki}^{\text{out}})(r_i(t))^2}{\Delta_k^{\text{out}}}, \quad (7a)$$

$$\frac{\partial z_k(t)}{\partial \pi_{ki}^{\text{out}}} = -m_{ki}^{\text{out}} r_i(t) + \frac{\epsilon_k^{\text{out}}(t)((m_{ki}^{\text{out}})^2(1 - 2\pi_{ki}^{\text{out}}) - \Xi_{ki}^{\text{out}})(r_i(t))^2}{2\Delta_k^{\text{out}}}, \quad (7b)$$

$$\frac{\partial z_k(t)}{\partial \Xi_{ki}^{\text{out}}} = \frac{\epsilon_k^{\text{out}}(t)(1 - \pi_{ki}^{\text{out}})(r_i(t))^2}{2\Delta_k^{\text{out}}}. \quad (7c)$$

Next, we derive the learning equation for the hyper-parameters in the reservoir and input layer, i.e.,  $\theta_{ij} \equiv (m_{ij}, \pi_{ij}, \Xi_{ij})$  and  $\theta_{ij}^{\text{in}} \equiv (m_{ij}^{\text{in}}, \pi_{ij}^{\text{in}}, \Xi_{ij}^{\text{in}})$ . To get a general form, we set  $\tilde{m}_{ij} \equiv (m_{ij}, m_{ij}^{\text{in}})$ ,  $\tilde{\pi}_{ij} \equiv (\pi_{ij}, \pi_{ij}^{\text{in}})$ , and  $\tilde{\Xi}_{ij} \equiv (\Xi_{ij}, \Xi_{ij}^{\text{in}})$ . Based on the chain rule, we then arrive at the following equations,

$$\frac{\partial \mathcal{L}}{\partial \tilde{m}_{ij}} = \sum_{t=0}^T \frac{\partial \mathcal{L}}{\partial h_i(t)} \frac{\partial h_i(t)}{\partial u_i(t)} \frac{\partial u_i(t)}{\partial \tilde{m}_{ij}} = \sum_{t=0}^T \alpha \delta_i(t) \frac{\partial u_i(t)}{\partial \tilde{m}_{ij}}, \quad (8a)$$

$$\frac{\partial \mathcal{L}}{\partial \tilde{\pi}_{ij}} = \sum_{t=0}^T \frac{\partial \mathcal{L}}{\partial h_i(t)} \frac{\partial h_i(t)}{\partial u_i(t)} \frac{\partial u_i(t)}{\partial \tilde{\pi}_{ij}} = \sum_{t=0}^T \alpha \delta_i(t) \frac{\partial u_i(t)}{\partial \tilde{\pi}_{ij}}, \quad (8b)$$

$$\frac{\partial \mathcal{L}}{\partial \tilde{\Xi}_{ij}} = \sum_{t=0}^T \frac{\partial \mathcal{L}}{\partial h_i(t)} \frac{\partial h_i(t)}{\partial u_i(t)} \frac{\partial u_i(t)}{\partial \tilde{\Xi}_{ij}} = \sum_{t=0}^T \alpha \delta_i(t) \frac{\partial u_i(t)}{\partial \tilde{\Xi}_{ij}}, \quad (8c)$$

where we have defined  $\delta_i(t) \equiv \frac{\partial \mathcal{L}}{\partial h_i(t)}$ . The auxiliary variable  $\delta_i(t)$  can be computed by the chain rule once again, resulting in a BPTT equation of the error signal starting from the last time-step  $T$ :

$$\delta_i(t) = \sum_j \frac{\partial \mathcal{L}}{\partial h_j(t+1)} \frac{\partial h_j(t+1)}{\partial h_i(t)} + \sum_k \frac{\partial \mathcal{L}}{\partial z_k(t)} \frac{\partial z_k(t)}{\partial r_i(t)} \phi'(h_i(t)), \quad (9)$$

where  $t = 0, 1, 2, \dots, T-1$ , and  $\phi'(\cdot)$  denotes the derivative of the transfer function. The first summation in  $\delta_i(t)$  can be directly expanded as

$$\sum_j \frac{\partial \mathcal{L}}{\partial h_j(t+1)} \frac{\partial h_j(t+1)}{\partial h_i(t)} = (1 - \alpha)\delta_i(t+1) + \sum_j \alpha \delta_j(t+1) \frac{\partial u_j(t+1)}{\partial h_i(t)}, \quad (10a)$$

$$\frac{\partial u_j(t+1)}{\partial h_i(t)} = \frac{\partial u_j(t+1)}{\partial r_i(t)} \frac{\partial r_i(t)}{\partial h_i(t)} = (1 - \pi_{ji})m_{ji}\phi'(h_i(t)) + \epsilon_j^u(t+1) \frac{(\varrho_{ji} - (\mu_{ji})^2)r_i(t)\phi'(h_i(t))}{\sqrt{((\Delta_j^{\text{in}}(t+1))^2 + (\Delta_j^{\text{rec}}(t))^2)}}. \quad (10b)$$

The second summation in  $\delta_i(t)$  is given by

$$\sum_k \frac{\partial \mathcal{L}}{\partial z_k(t)} \frac{\partial z_k(t)}{\partial h_i(t)} = \sum_k \frac{\partial \mathcal{L}}{\partial z_k(t)} \times \left[ \mu_{ki}^{\text{out}} + \epsilon_k^{\text{out}}(t) \frac{(\varrho_{ki}^{\text{out}} - (\mu_{ki}^{\text{out}})^2) r_i(t)}{\Delta_k^{\text{out}}(t)} \right] \phi'(h_i(t)). \quad (11)$$

It is worth noting that for the last time-step  $T$ , the error signal  $\delta_i(T)$  is written as

$$\delta_i(T) = \sum_k \frac{\partial \mathcal{L}}{\partial z_k(T)} \times \left[ \mu_{ki}^{\text{out}} + \epsilon_k^{\text{out}}(T) \frac{(\varrho_{ki}^{\text{out}} - (\mu_{ki}^{\text{out}})^2) r_i(T)}{\Delta_k^{\text{out}}(T)} \right] \phi'(h_i(T)). \quad (12)$$

To compute Eq. (8), we need to work out the following derivatives, which characterize the sensitivity of the pre-activation under the change of hyper-parameters  $\theta_{ij}$  and  $\theta_{ij}^{\text{in}}$ . We summarize the results as follows,

$$\frac{\partial u_i(t)}{\partial m_{ij}^{\text{in}}} = (1 - \pi_{ij}^{\text{in}}) x_j(t) + \epsilon_i^{\text{u}}(t) \frac{\mu_{ij}^{\text{in}} \pi_{ij}^{\text{in}} (x_j(t))^2}{\sqrt{(\Delta_i^{\text{in}}(t))^2 + (\Delta_i^{\text{rec}}(t-1))^2}}, \quad (13a)$$

$$\frac{\partial u_i(t)}{\partial \pi_{ij}^{\text{in}}} = -m_{ij}^{\text{in}} x_j(t) + \epsilon_i^{\text{u}}(t) \frac{((m_{ij}^{\text{in}})^2 (1 - 2\pi_{ij}^{\text{in}}) - \Xi_{ij}^{\text{in}}) (x_j(t))^2}{2\sqrt{(\Delta_i^{\text{in}}(t))^2 + (\Delta_i^{\text{rec}}(t-1))^2}}, \quad (13b)$$

$$\frac{\partial u_i(t)}{\partial \Xi_{ij}^{\text{in}}} = \epsilon_i^{\text{u}}(t) \frac{(1 - \pi_{ij}^{\text{in}}) (x_j(t))^2}{2\sqrt{(\Delta_i^{\text{in}}(t))^2 + (\Delta_i^{\text{rec}}(t-1))^2}}, \quad (13c)$$

$$\frac{\partial u_i(t)}{\partial m_{ij}} = (1 - \pi_{ij}) r_j(t-1) + \epsilon_i^{\text{u}}(t) \frac{\mu_{ij} \pi_{ij} (r_j(t-1))^2}{\sqrt{(\Delta_i^{\text{in}}(t))^2 + (\Delta_i^{\text{rec}}(t-1))^2}}, \quad (13d)$$

$$\frac{\partial u_i(t)}{\partial \pi_{ij}} = -m_{ij} r_j(t-1) + \epsilon_i^{\text{u}}(t) \frac{((m_{ij})^2 (1 - 2\pi_{ij}) - \Xi_{ij}) (r_j(t-1))^2}{2\sqrt{(\Delta_i^{\text{in}}(t))^2 + (\Delta_i^{\text{rec}}(t-1))^2}}, \quad (13e)$$

$$\frac{\partial u_i(t)}{\partial \Xi_{ij}} = \epsilon_i^{\text{u}}(t) \frac{(1 - \pi_{ij}) (r_j(t-1))^2}{2\sqrt{(\Delta_i^{\text{in}}(t))^2 + (\Delta_i^{\text{rec}}(t-1))^2}}. \quad (13f)$$

In this learning process, our model learns a RNN ensemble to realize the time-dependent computation, in contrast to the standard BPTT algorithm which gives only a point-estimate of RNN weights. In particular, if we set  $\pi = 0$  and  $\Xi = 0$ , our learning equation reduces to the standard BPTT. Hence, our model can be thought of as a generalized version of BPTT (i.e., gBPTT), as shown in Fig. 2, where each weight parameter should be understood as the SaS hyper-parameters, corresponding to our ensemble setting.

The size of the candidate network space can be captured by the network entropy  $S = -\int_{\mathbb{R}^{\mathcal{D}}} P(\mathbf{w}) \ln P(\mathbf{w}) d\mathbf{w}$ , where  $\mathcal{D}$  is the number of weight parameters in the network. If we assume the joint distribution of weights to be factorized across individual connections, the overall energy  $S$  can be obtained by summing up the entropy of individual weights as  $S = \sum_{\ell} S_{\ell}$ . The entropy of each directed connection  $\ell$  is derived as follows [13]:

$$S_{\ell} = -\pi_{\ell} \ln [\pi_{\ell} \delta(0) + (1 - \pi_{\ell}) \mathcal{N}(0|m_{\ell}, \Xi_{\ell})] - \frac{1 - \pi_{\ell}}{\mathcal{B}} \sum_s \Gamma(\epsilon_s), \quad (14)$$

where  $\Gamma(\epsilon_s) = \ln [\pi_{\ell} \delta(m_{\ell} + \sqrt{\Xi_{\ell}} \epsilon_s) + \frac{1 - \pi_{\ell}}{\sqrt{\Xi_{\ell}}} \mathcal{N}(\epsilon_s|0, 1)]$  and  $\mathcal{B}$  denotes the number of standard Gaussian variables  $\epsilon_s$ . This model entropy is just an approximate estimate of the true value whose exact computation is impossible.

If  $\pi_{\ell} = 0$ , the probability distribution of  $w_{\ell}$  can be written as  $P(w_{\ell}) = \mathcal{N}(w_{\ell}|m_{\ell}, \Xi_{\ell})$ , and the entropy  $S_{\ell}$  can be analytically computed as  $\frac{1}{2} \ln(2\pi e \Xi_{\ell})$ . If  $\Xi_{\ell} = 0$ , the Gaussian distribution reduces to a Dirac delta function, and the entropy becomes an entropy of discrete random variables,  $S_{\ell} = \pi_{\ell} \ln \pi_{\ell} + (1 - \pi_{\ell}) \ln(1 - \pi_{\ell})$ . However, there may exist a mixture of discrete and continuous contributions to the entropy. Therefore, the entropy value can take negative values. In practice, we use  $\delta(x) = \lim_{a \rightarrow 0^+} \frac{1}{\sqrt{2\pi a}} e^{-\frac{x^2}{2a}}$  to approximate the delta-peak with a small value of  $a$ . The stochasticity of the SaS distribution can be also decomposed into two levels: one at the choice of connection that is absent and the other at the Gaussian slab itself. The former one is a discrete entropy characterized by the spike probability, and the latter is a continuous entropy just characterized by the variance of the Gaussian slab.

### III. RESULTS

In this section, we show applications of our ensemble theory of temporal credit assignment to both engineering and computational cognitive tasks, i.e., pixel-by-pixel MNIST digit classification, and the multisensory integration demonstrating the benefit of multiple sources of information for decision making. We will explore in detail rich properties of trained RNN model accomplishing the above computational tasks of different nature.

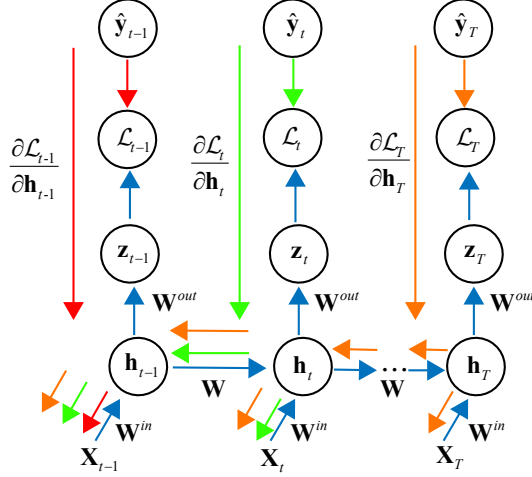


FIG. 2: Illustration of the generalized back-propagation through time.  $\mathbf{X}_t$  is a time-dependent input into the network, resulting in a sequence of hidden representations  $\mathbf{r}(t)$  (i.e.,  $\phi(\mathbf{h}_t)$ ) and a time-dependent loss  $\mathcal{L}_t$ . The error signal  $\frac{\partial \mathcal{L}_t}{\partial \mathbf{h}_t}$  propagates back from the last time-step  $T$  to the first time step, yielding the temporally accumulated gradients for hyper-parameters to be updated. The contribution of  $\frac{\partial \mathcal{L}_t}{\partial \mathbf{z}_t}$  is not shown in this plot.  $\mathbf{X}_t$ ,  $\mathbf{z}_t$  and  $\mathbf{h}_t$  indicate  $\mathbf{x}(t)$ ,  $\mathbf{z}(t)$  and  $\mathbf{h}(t)$  in the main text, respectively.

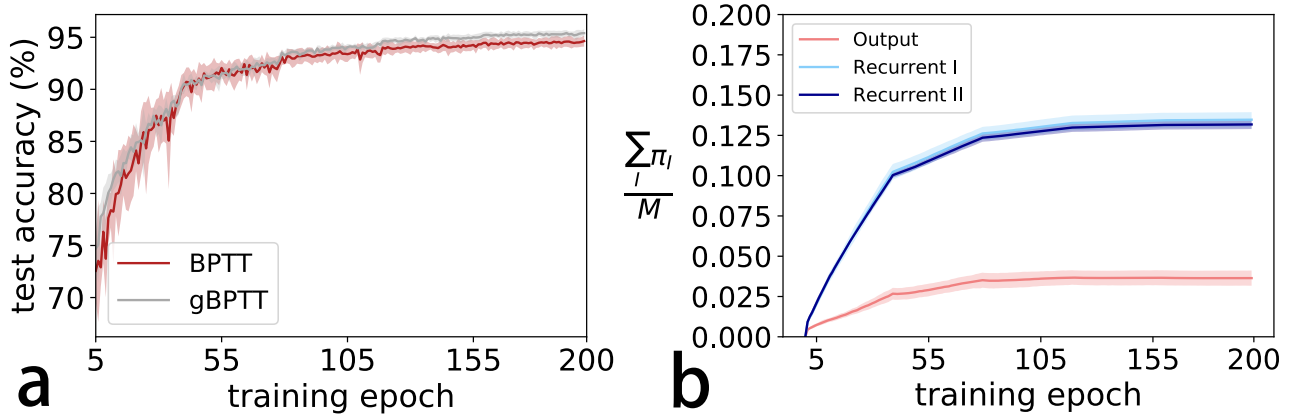


FIG. 3: Properties of trained RNN models for the pixel-by-pixel MNIST classification. (a) Test accuracy versus training epoch. The network of  $N = 100$  neurons is trained on the full MNIST dataset (60 000 images), and tested on the unseen data of 10 000 images. Five independent runs of the algorithm are considered. There are no baseline inputs. Other parameters for training are as follows:  $\alpha = 0.1$ ,  $\ell_2$  regularization strength is  $10^{-4}$ , and the initial learning rate  $\text{lr}_0 = 0.001$ . (b) Evolution of the network sparsity per connection. Recurrent I denotes the case of  $w_{ij}$  ( $i < j$ ) along which the recurrent feedback passes from neuron  $j$  to neuron  $i$ ; while recurrent II denotes the case of  $w_{ji}$  ( $j > i$ ) along which the recurrent feedback passes from neuron  $i$  to neuron  $j$ . The fluctuation is estimated from five independent runs [the same training conditions as in (a)].

### A. Pixel-by-Pixel MNIST digit classification

Training RNNs is hard because of long-term dependency in the sequence of inputs. A challenging task of long-term dependency is to train a RNN to classify the MNIST images when the 784 pixels are fed into the network one by one (note that  $\mathbf{x}_0 = 0$ ), where the network is required to predict the category of the image after seeing all the 784 pixels. This task displays a long range of dependency, because the network reads one pixel at a single time-step in a scan-line order from the top left pixel to the bottom right pixel (Fig. 5), and the information of as long as 784 time steps must be maintained before the final decision. We apply the vanilla RNN with  $N = 100$  recurrent units to achieve this challenging goal. Because the input size is one in this task, and thus the set of hyper-parameters  $(\pi^{\text{in}}, \Xi^{\text{in}})$  are set to zero (i.e., the deterministic limit). The entire MNIST dataset is divided into mini-batches for stochastic gradient descent, and we apply cross entropy as the objective function to be minimized. In this task, the

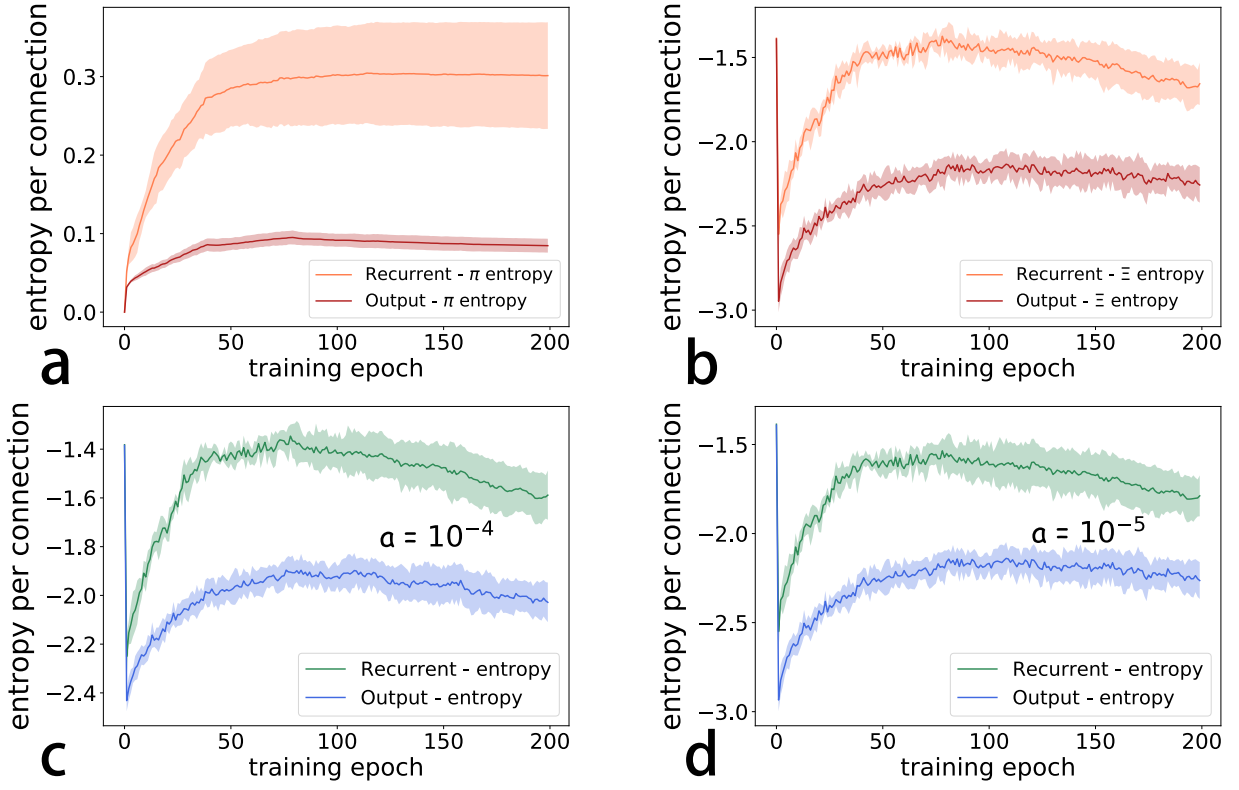


FIG. 4: Evolution of entropy per connection for the pixel-by-pixel MNIST classification. The training conditions are the same as in Fig. 3. Five independent runs are considered. The input weight is deterministic without any stochasticity. In addition, to avoid divergence, we relax all values of  $\Xi$  smaller than  $a$  to be  $a$  in the computation of the entropy. Our results are not sensitive to the choice of  $a$ , once the value of  $a$  is small. (a,b) We decompose the variability of the SaS distribution into two levels: the variability of selecting zero synapses ( $\pi$ -entropy) and the variability inside the Gaussian slab ( $\Xi$ -entropy). (c,d) Evolution of entropy per connection ( $\mathcal{B} = 100$ ). We use the Gaussian distribution of small variance (indicated by  $a$ ) to approximate the delta-peak. The value of  $a$  does not affect the qualitative behavior of the entropy profile.

error signal appears only after the network reads all the 784 pixels. In the current setting, we ignore the noise terms in the dynamics equations [Eq. (1) and Eq. (2)]. Surprisingly, although working at the ensemble level, our model can achieve a comparable or even better performance than the traditional BPTT method, as shown in Fig. 3 (a).

Our simulation reveals that the sparsity per connection,  $\frac{\sum_i \pi_i}{M}$  (a total of  $M$  directed connections in the network), achieves a larger value in the recurrent layer compared with the output layer; this behavior does not depend on the specific directions of the coupling [Fig. 3 (b)]. During training, the sparsity level grows until saturation, suggesting that the training may remove or minimize the impacts of irrelevant information across time steps. Interestingly, the entropy per connection in the recurrent layer also increases at the early stage of the training, but decreases at the late stage [Fig. 4], showing that the training is able to reorganize the information landscape shaped by the recurrent feedbacks. The network at the end of training becomes more deterministic (e.g.,  $\Xi$  gets close to zero, or the spike probability goes away from one half). The discrete  $\pi$ -entropy always increases until saturation at a certain level. The entropy profile in the output layer shows a similar behavior yet with a lower entropy value. This is consistent with distinct roles of recurrent and readout layers. The recurrent layer (or computing reservoir) searches for an optimal way of processing temporally complex sensory inputs, while the output layer implements the decoding of the signals hidden in the reservoir dynamics. Note that two types of deterministic weights yield vanishing individual entropy values, i.e., (i)  $\pi = 1$  (unimportant (UIP) weight); (ii)  $\pi = 0$  and  $m \neq 0$  (very important (VIP) weight).

To study the network behavior from the perspective of hyper-parameter distributions, we plot the distribution of three sets of parameters ( $\mathbf{m}, \Xi, \pi$ ) for the output layer, two different directions of connections in the recurrent layer, and  $\mathbf{m}$  of the input layer ( $(\pi^{\text{in}}, \Xi^{\text{in}})$  are set to zero as explained before), as shown in Fig. 5. The distribution of spike probability  $\pi$  has the shape of  $L$  for all layers. The extreme at  $\pi = 0$  indicates that the corresponding synaptic weight carries important feature-selective information, and are thus critical to the network performance. The shape of  $\pi$ -distribution profile reflects the task difficulty for the considered network (given the same initialization condition), since we observe that in a simpler task for the network to read 28 pixels at each time step (rather than one pixel by

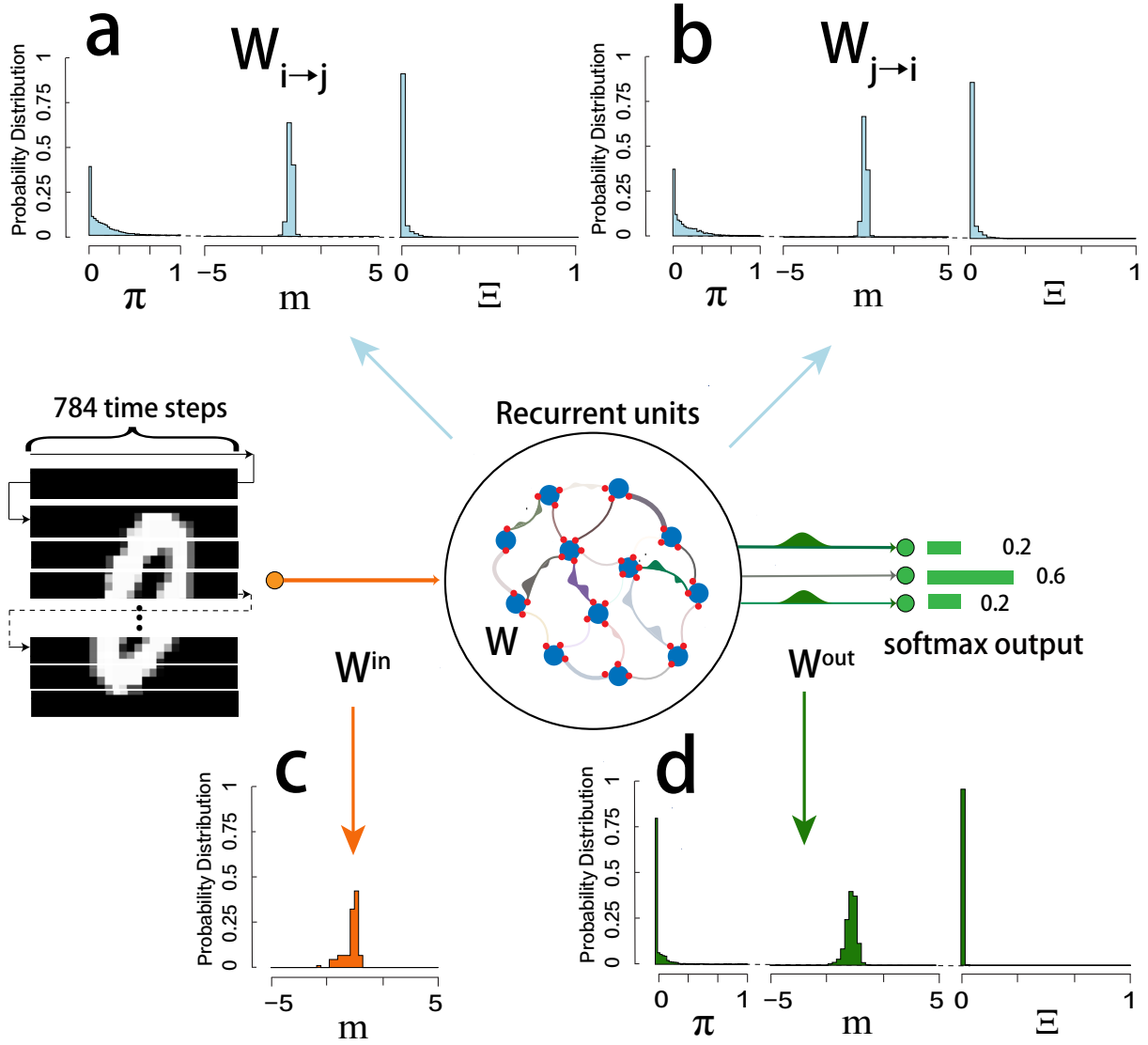


FIG. 5: Distributions of hyper-parameters  $(\pi, m, \Xi)$  in the trained network (pixel-by-pixel MNIST classification). The training conditions are the same as in Fig. 3. In (a,b),  $i < j$  is assumed.

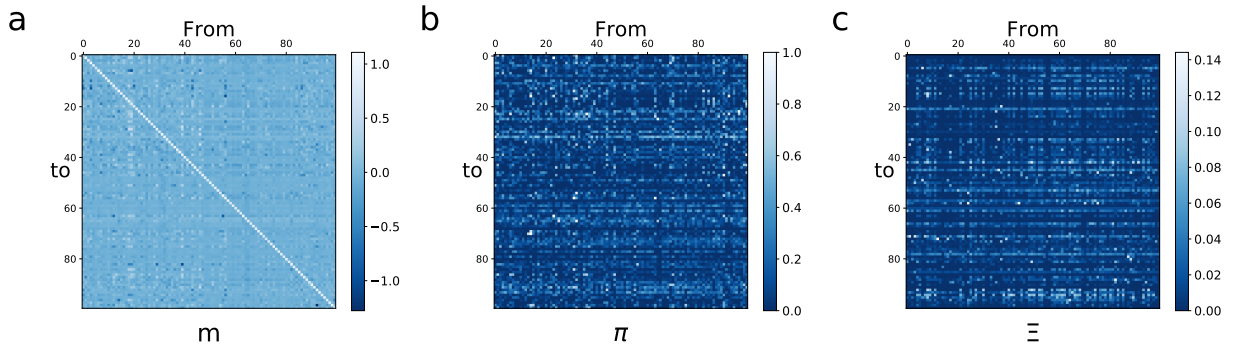


FIG. 6: Heterogeneous structures of trained RNN networks. Training conditions are the same as in Fig. 3. Hyper-parameters  $(\pi, m, \Xi)$  are plotted in the matrix form with the dimension  $N \times N$ , where  $N$  indicates the number of recurrent neurons. The element of these matrices, say  $m_{ij}$ , denotes the hyper-parameter value for the directed link from neuron  $j$  to neuron  $i$ .



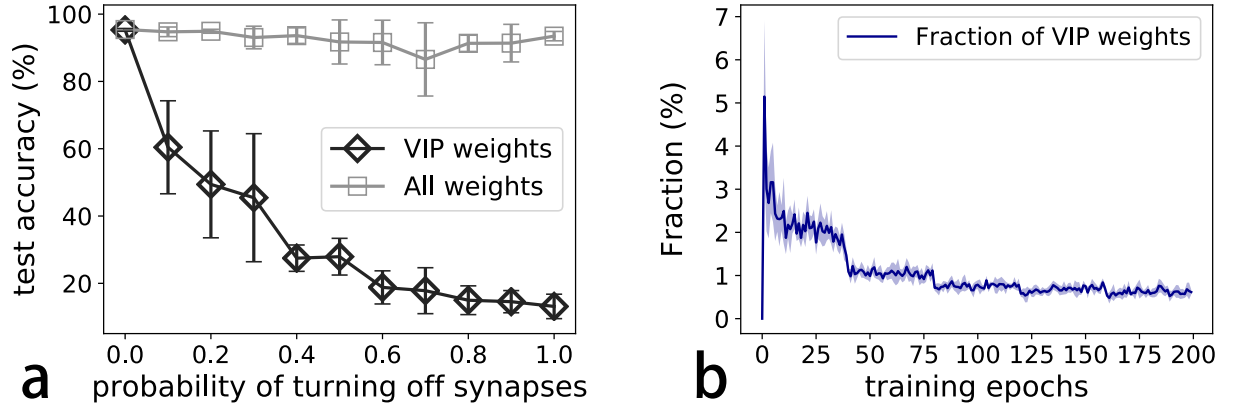


FIG. 7: Targeted weight perturbation in the recurrent layer of RNNs. All the training conditions are kept the same as in Fig 3, and the results are averaged over five independent runs. (a) VIP weights are stochastically turn off, and the same number of randomly selected weights from the entire weight population are also deleted for comparison of the resultant performance. (b) The fraction of VIP weights changes during the training process.

one pixel), the profile of  $\pi$ -distribution develops a U shape, with the other peak at  $\pi = 1$ , implying the emergence of a significant fraction of UIP weights. In addition,  $\Xi$  has an L-shaped distribution which peaks at zero, suggesting that the corresponding weight distribution takes a deterministic value of  $m$ , which becomes the weight value of that connection.

As for the readout layer, the mean of the continuous slab becomes much more dispersed, compared with that of the recurrent layer, while the statistics profile for  $\pi$  and  $\Xi$  becomes more converged, which is in an excellent agreement with the entropy profile shown in Fig. 4. We thus conclude that the recurrent layer has a greater variability than the output layer. This great variability allows the recurrent layer to transform the complex sensory inputs with hierarchical spatiotemporal structures in a flexible way. Nevertheless, the minimal variability makes the readout behavior more robust. It is therefore interesting in future works to address the precise mechanism underlying how the statistics of the connections in a RNN facilitates the formation of latent dynamics for computation.

We next look at the specific profile of individual hyper-parameters in a matrix form (Fig. 6). We find that the diagonal (self-interaction) of  $m$  emerges from gBPTT (note that the diagonals of  $\pi$  and  $\Xi$  nearly vanish), demonstrating the significant role of self-interactions in maintaining long-term memory and thereby the learning performance, in accord with the heuristic strategy used in a recent study [19]. There also appears heterogeneity in the hyper-parameter matrices, i.e., some directed connections play a more important role than the others. In particular, some connections can be eliminated for saving computation resources.

Our method can identify the exact nature of each directed connection in the network. Targeted weight perturbation can thus be performed in the recurrent layer (Fig. 7). In the course of training, the fraction of VIP connections slowly decreases, although the fraction of VIP connections is not significant (around 1%) [Fig. 7(b)]. Surprisingly, pruning these VIP weights could strongly deteriorate the test performance of the network (up to the chance level), whereas pruning the same number of randomly selected connections from the entire weight population yields a negligible drop of the test accuracy. We thus conclude that in a RNN, there exists a minority of VIP weights carrying key spatiotemporal information essential for decision making of the network.

We then explore whether the selectivity of neurons for the sensory inputs could emerge from our training. The degree of selectivity for an individual unit, say neuron  $i$ , can be characterized by an index, namely SLI [23] as follows

$$\text{SLI}(i) = \frac{1}{1 - \frac{1}{N_s}} \left[ 1 - \frac{\left( \frac{1}{N_s} \sum_{s=1}^{N_s} r_{i,s} \right)^2}{\frac{1}{N_s} \sum_{s=1}^{N_s} (r_{i,s})^2} \right], \quad (15)$$

where  $r_{i,s}$  indicates the response of the neuron to the input stimulus  $s$  with the total number of stimulus-class being  $N_s$  ( $N_s = 10$  in the MNIST experiment). Note that  $r_{i,s}$  for the RNN depends on the time step as well. The value of SLI ranges from 0 (when the neuron responds identically to all stimuli) to 1 (when the neuron responds only to a single stimulus), and a higher SLI indicates a higher degree of selectivity, and vice versa. Interestingly, we find that most neurons have mixed selectivity shown in Fig. 8 (the right panel), whose SLI lies between 0 and 1, and such neurons respond strongly to a few types of images. The mixed selectivity was also discovered in complex cognitive tasks [24]. We also observe that some neurons are particularly selective to only one type of images with a high value of SLI [Fig. 8 (middle)], while the remaining part of neurons keeps silent with an SLI near to zero [Fig. 8 (left)]. As

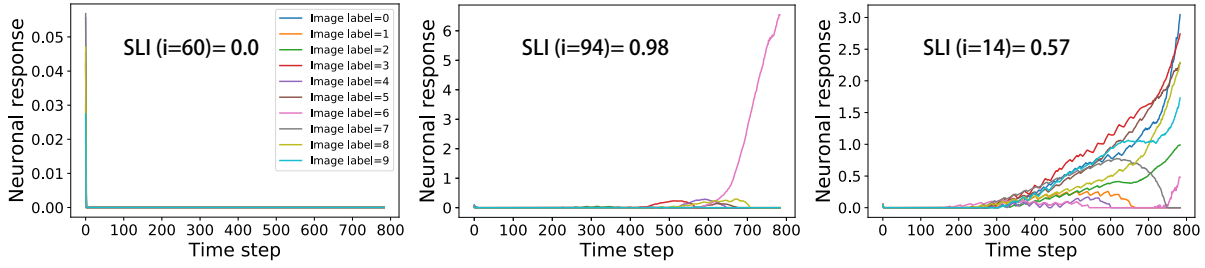


FIG. 8: Selectivity of representative neurons in RNNs learning MNIST digit classification. (Left) the non-selectivity case. (Middle) the uni-selectivity case. (Right) the mixed-selectivity case. Time steps indicate the dynamic steps during the test phase, and the labels in the left panel are shared for the other two panels.

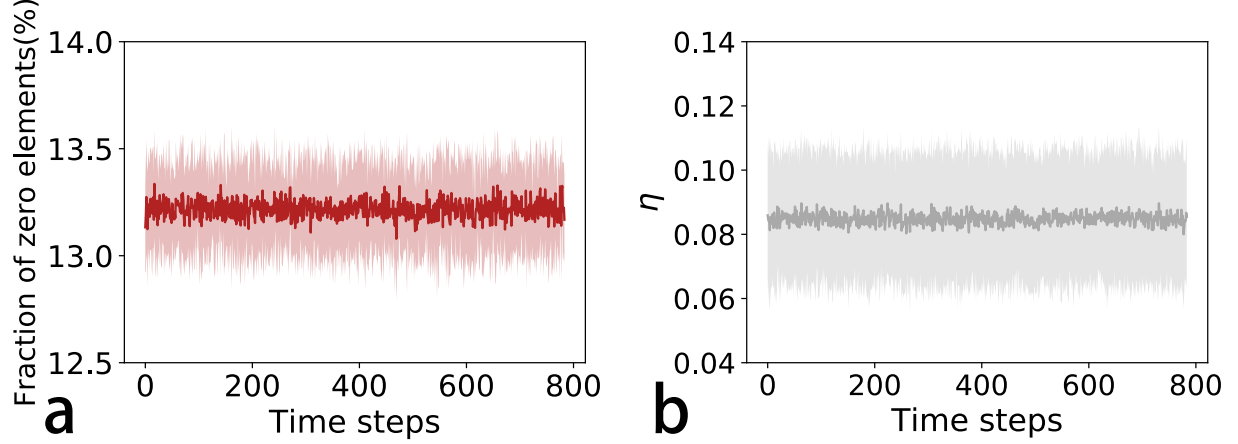


FIG. 9: The statistics of time-dependent networks does not change significantly. (a) The fraction of zero elements of sampled weights across 784 time steps. The fluctuation is computed from five independent runs. (b) The asymmetry measure  $\eta$  defined by  $\frac{\overline{w_{ij}w_{ji}}}{\overline{w_{ij}^2}}$  versus time step. The over-bar means the average over all reciprocal connections. The result is averaged over five independent runs.

expected, the selectivity property emerges slightly before the decision making of the network.

We finally remark that gBPTT produces a network ensemble, characterized by the hyper-parameter set of the SaS distribution. A concrete network can thus be sampled from this ensemble. During training, we use independently time-dependent Gaussian noise  $\epsilon^u(t)$  to approximate the statistics of the ensemble. Accordingly, we find that a time-dependent concrete network yields the identical test performance with the mean-field propagation (i.e., using the parametrized pre-activation, see Eq. (4)). The overall statistics of sampled networks does not vary significantly across dynamic steps (Fig. 9). This observation is in stark contrast to the traditional RNN training, where a deterministic weight matrix is used in all time steps. In fact, in a biological neural circuit, changes in synaptic connections are essential for the development and function of the nervous system [25, 26]. In other words, the specific details of the connection pattern for a circuit may not be critical to the behavior, but rather, the parameters underlying the statistics of weight distributions become dominant factors for the behavioral output of the network (see also a recent paper demonstrating that innate face-selectivity could emerge from statistical variation of the feedforward projections in hierarchical neural networks [27]). Therefore, our current ensemble perspective of training RNNs offers a promising framework to achieve neural computation with a dynamic network, which is likely to be consistent with biologically plausible computations with fluctuating dendritic spines, e.g., dendritic spines can undergo morphological remodeling in adaptation to sensory stimuli or in learning [26].

## B. Multisensory integration task

Multisensory integration is a fundamental ability of the brain to combine cues from multiple senses to form robust perception of signals in the noisy world [16, 17]. In typical cognitive experiments, two separate sources of information

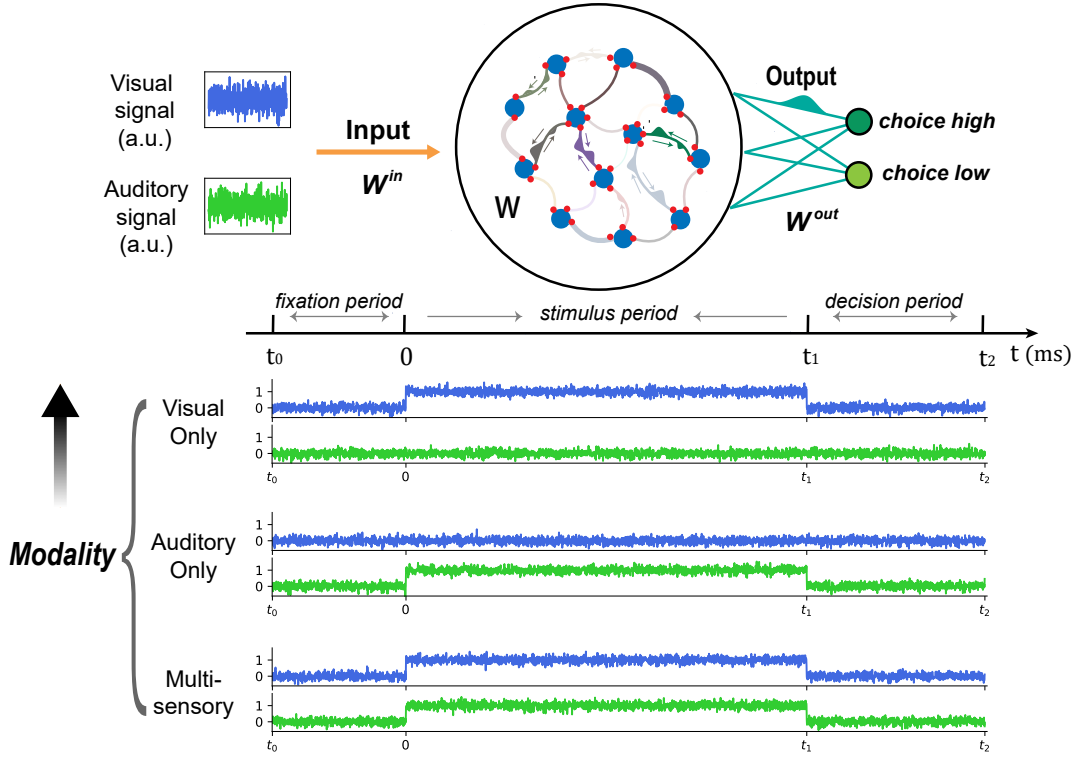


FIG. 10: Schematic illustration of the RNN performing a multi-sensory integration task. In one trial, the task consists of three consecutive stages (of lengths 300, 900, and 400 ms, respectively) including a fixation period ( $t_0 \sim 0$ ), a stimulus period ( $0 \sim t_1$ ), and a decision period ( $t_1 \sim t_2$ ). Note that in a test trial, the lengths of three stages are 500, 1000, and 300 ms, respectively. During the fixation period, the network must maintain a low output value, ensuring that the network will be sensitive to the stimulus signals. During the stimulus period, either or both (or multisensory) sources of signals with the same frequency  $f$ , including visual signal and auditory signal, act as the input to the network. The frequency  $f$  ranges from 9 to 16. Each type of sensory input contains positively tuned and negatively tuned signals (only the positively tuned one is shown in the plot). During the decision period, there are no modality input signal, and the network must learn to discriminate the even rate of the stimulus period, i.e., the output must hold a high or low value correctly. The output at the last time step of the decision period is assigned the final decision of one trial. Other parameters for training are as follows:  $x_0 = 0.2$  for all neurons,  $\tau = 100$  ms,  $\alpha = 0.2$ ,  $\sigma = 0.15$ ,  $\sigma_{in} = 0.01$ ,  $\ell_2$  regularization strength is  $10^{-3}$ , and the initial learning rate  $lr_0 = 0.001$ .  $\Delta t = 0.5$  ms for testing.

are provided to animals, e.g., rats, before the animals make a decision. The source of information can be either auditory clicks or visual flashes, or both [28]. When the task becomes difficult, the multisensory training is more effective than the unisensory one. Akin to animals trained to perform a behavior task, RNNs can also learn the input-output mapping through an optimization procedure, which is able to provide a quantitative way to understand the computational principles underlying the multisensory integration. In particular, by increasing biological plausible levels of network architectures and even learning dynamics [8, 10], one may generate quantitative hypotheses about the dynamical mechanisms that may be implemented in real neural circuits to solve the same behavior task. In this section, we restrict the network setting to the simplest case, i.e., a group of neurons are reciprocally connected with continuous firing rate dynamics. To consider more biological details is straightforward, e.g., taking Dale's principle [21]. The goal in this section is to show that our ensemble perspective also works in modeling cognitive computational tasks.

In the multisensory integration experiment (MSI), either or both of auditory and visual signals are fed into the recurrent network via deterministic weights (the same reason as in pixel-by-pixel MNIST task), which is required, after a stimulus period, to report whether the frequency of the presented stimulus is above a decision boundary (12.5 events per second)(see Fig. 10). One third of network units receive only visual input, while another third receive only auditory input, and the remaining third do not receive any input. The continuous variable  $r(t)$  in our model is an activity vector indicating the firing rates of neurons, obtained through a non-linear transfer function (ReLU here) of the synaptic current input  $[h(t)]$ . The current includes both of external input and recurrent feedback. The output  $z(t)$  is a weighted readout of the neural responses in the reservoir (a binary choice for the MSI task). The RNN is used here to model the multisensory event-rate discrimination task for the rats [21, 28], and is trained by our gBPTT

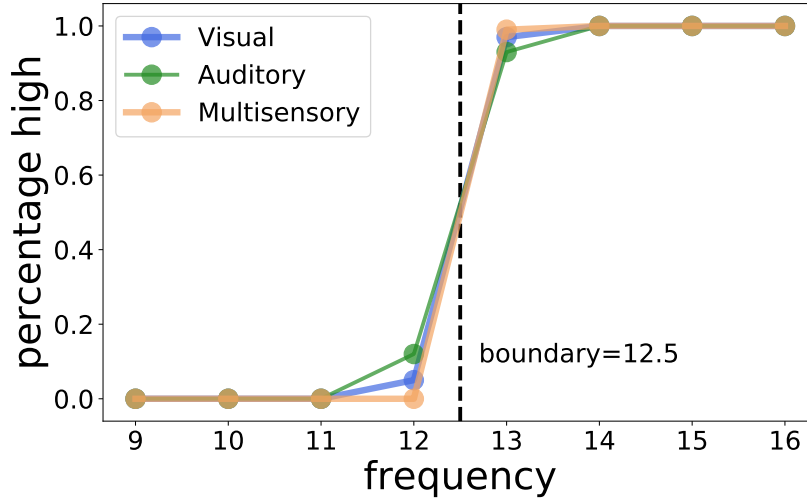


FIG. 11: Psychometric function for the MSI task. This function shows the percentage of high choices made by the network as a function of the event rate for both unisensory and multisensory trials. Each marker is the mean result over 100 independent test trials. Other training conditions are the same as in Fig. 10.

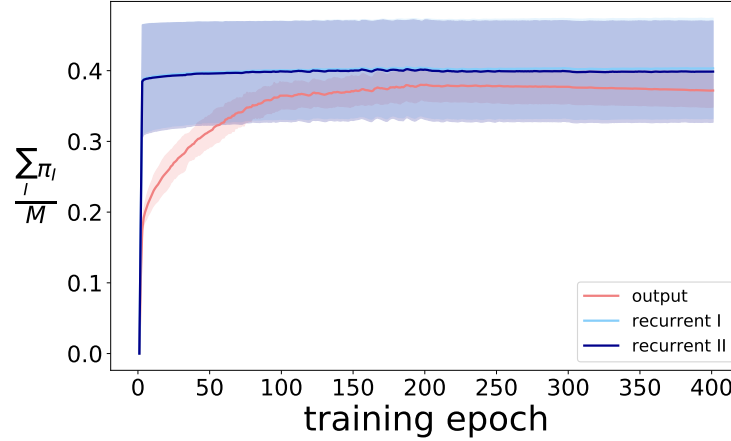


FIG. 12: Evolution of sparsity densities with training epochs for the MSI task. The lines are the mean results of ten independent training trials, and the shadow indicates the fluctuation. Recurrent I and II are the lower and upper triangles of the  $\pi$  matrix, respectively. Other training conditions are the same as in Fig. 10.

to solve the same audiovisual integration task. The visual and auditory inputs can be either positively (increasing function of event rate) or negatively tuned (decreasing function of event rate). Showing the network both types of tuned inputs could improve the training [29]. The RNN is composed of 150 neurons, whose recurrent dynamics is required to hold a high output value if the input event rate (represented by time-dependent noisy inputs) was above the decision boundary, and hold a low output value otherwise. Neurons are reciprocally connected, and the global statistics of the topology is learned from the training trials.

The benefits of multisensory inputs, as known in cognitive science [16], are reproduced by our RNN model trained by gBPTT (Fig. 11). Integrating multiple sources of information, rather than unisensory inputs, helps decision making particularly when the task becomes hard (i.e., around the decision boundary). As the training proceeds, the sparsity of the recurrent layer grows rapidly until saturation, while the sparsity of the output layer grows in the same manner but finally reaching a lower value yet with a small fluctuation (Fig. 12). The recurrent layer becomes sparser with training, demonstrating that the latent dynamics is likely low dimensional, because of existence of some unnecessary degrees of freedom in recurrent feedbacks. In contrast, the goal of the output layer is to decode the recurrent dynamics, and the output layer should therefore keep all relevant dimensions of information integrated, which requires a densely connected output layer. This behavior is consistent with the evolution of the entropy profile. The recurrent layer maintains a relatively higher level of variability, compared with that of the output layer at the end of training (see the

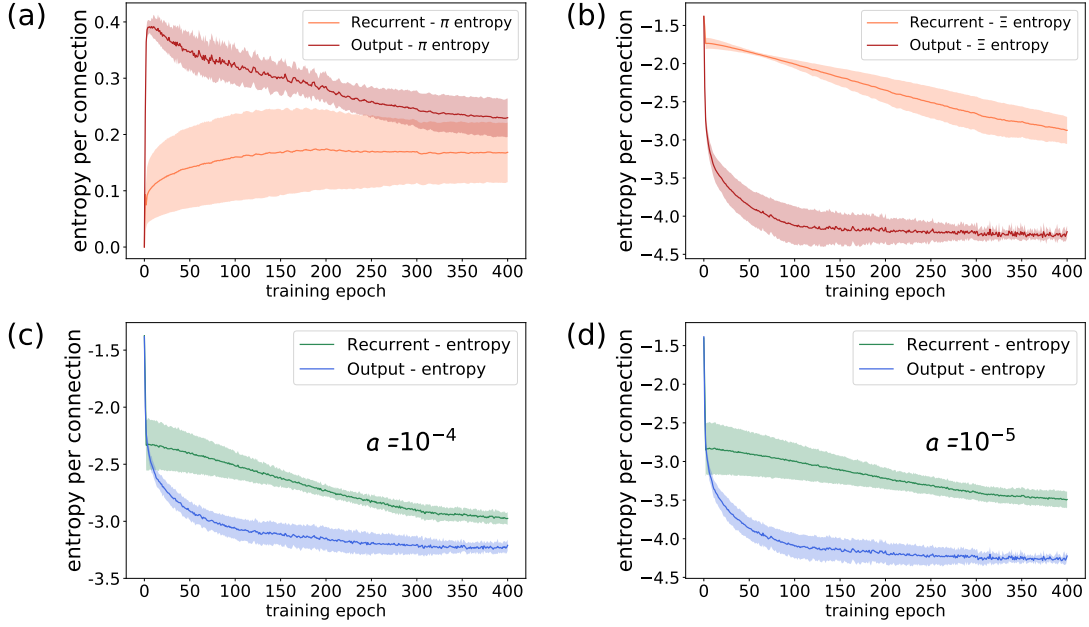


FIG. 13: Evolution of entropy densities with training epochs for the MSI task. The lines are the mean results of ten independent training trials, and the shadow indicates the fluctuation. The definitions of entropies are the same as in the MNIST experiment (see Fig. 4). The value of  $a$  does not affect the qualitative behavior of the entropy profile. Other training conditions are the same as in Fig. 10.

continuous entropy computed according to Eq. (14), or the  $\Xi$ -entropy in Fig. 13). In addition, the discrete  $\pi$ -entropy decreases with training in the output layer, in contrast to the increasing behavior of the same type of entropy in the recurrent layer (Fig. 13).

Let us then look at the distribution profile of hyperparameters (Fig. 14). In the output layer, the distribution of  $\pi$  is U-shaped, and  $\Xi$  shows a sharp single peak at zero, which demonstrates that a dominant part of the weight distribution reduces to the Bernoulli distribution with two peaks at 0 and  $m \neq 0$  respectively. The observed less variability in weight values of the output layer is consistent with the decoding stability. In the recurrent layer, the profile of  $\pi$ -distribution is U-shaped, and the distribution profile of  $\Xi$  resembles an L shape. This implies that there emerge VIP and UIP connections in the network. Moreover, a certain level of variability is allowed for the weight values, making a flexible computation possible in the internal dynamics.

Next, we ask whether our training leads to the emergence of neural selectivity, which indeed exists in the prefrontal cortex of behaving animals [24]. The selectivity properties of neurons play a critical role in the complex cognitive ability. In our trained networks, we also find that neurons in the recurrent layer display different types of selectivity (Fig. 15). In other words, neurons become highly active for either of modality (visual or auditory) and choice (high or low), or both (mixed selectivity).

We then explore the detailed patterns of the hyper-parameter matrices, which conveys individual contributions of each connection to the behavioral performance. By inspecting the sparsity matrix [Fig. 16 (b)], one can identify both unnecessary ( $\pi = 1$ ) and important connections ( $\pi = 0$ ). We also find that, some neurons prefer receiving or sending information during the recurrent computation. An interpretation is that, the spatio-temporal information is divided into relevant and irrelevant parts; the relevant parts are maintained through sending preference, while the irrelevant parts are blocked through receiving preference.

Target weight perturbation experiments (Fig. 17) show that the VIP weights play a fundamental role in supporting the task accuracy reached by the recurrent computation. Our method can thus provide precise temporal credit assignment to the MSI task, which the standard BPTT could not.

Finally, we remark that a dynamic network with time-dependent specified weight values is able to reach an equivalent accuracy with the network using the mean-field propagation. Note that the overall statistics of the network does not change significantly (Fig. 18), suggesting that the hyperparameters for the the weight statistics are more important than precise values of weights. In fact, dendritic spines in neural circuits, biological substrates for synaptic contacts, are also subject to fluctuation, i.e., a highly dynamic structure [25, 26]. Future exploration of this interesting connection would be fruitful, as an ensemble perspective is much more abstract than a concrete topology, while the specified stationary topology is still widely used in modern machine learning. Therefore, the ensemble perspective yielding a

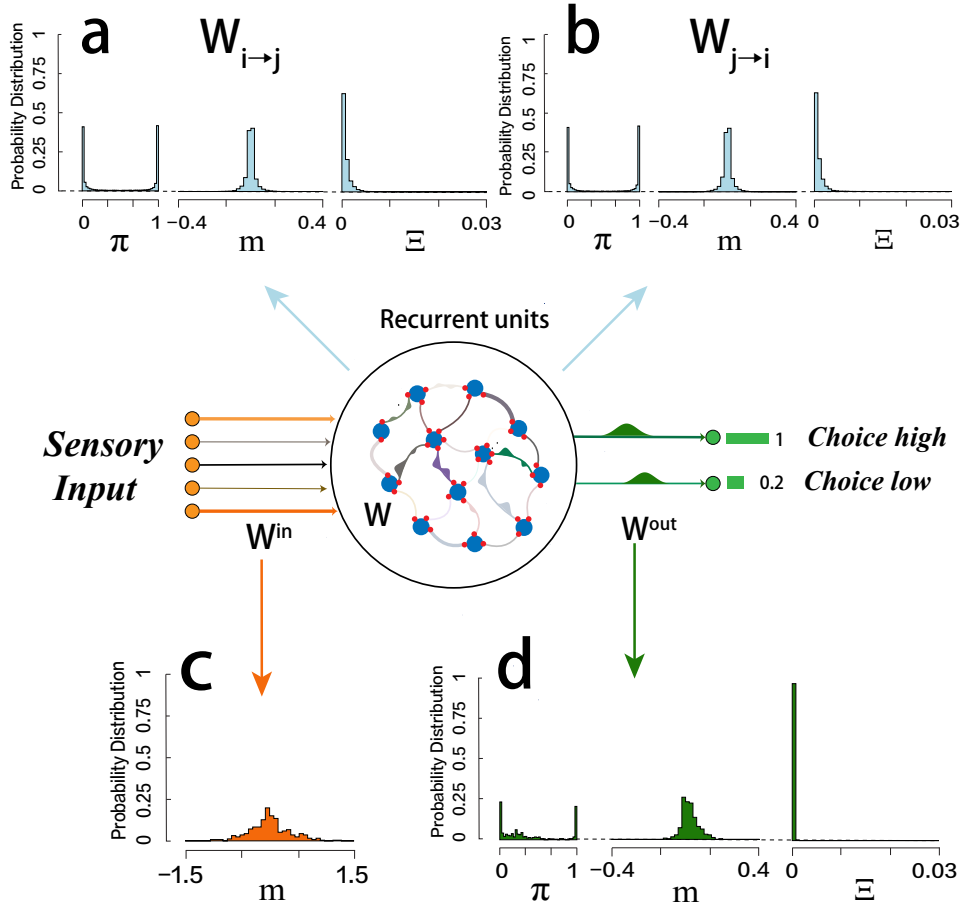


FIG. 14: Distributions of hyper-parameters ( $\pi$ ,  $m$ ,  $\Xi$ ) in input, recurrent and output layers of the RNN model for the MSI task. Training conditions are the same as in Fig. 10. In (a,b),  $i < j$  is assumed.

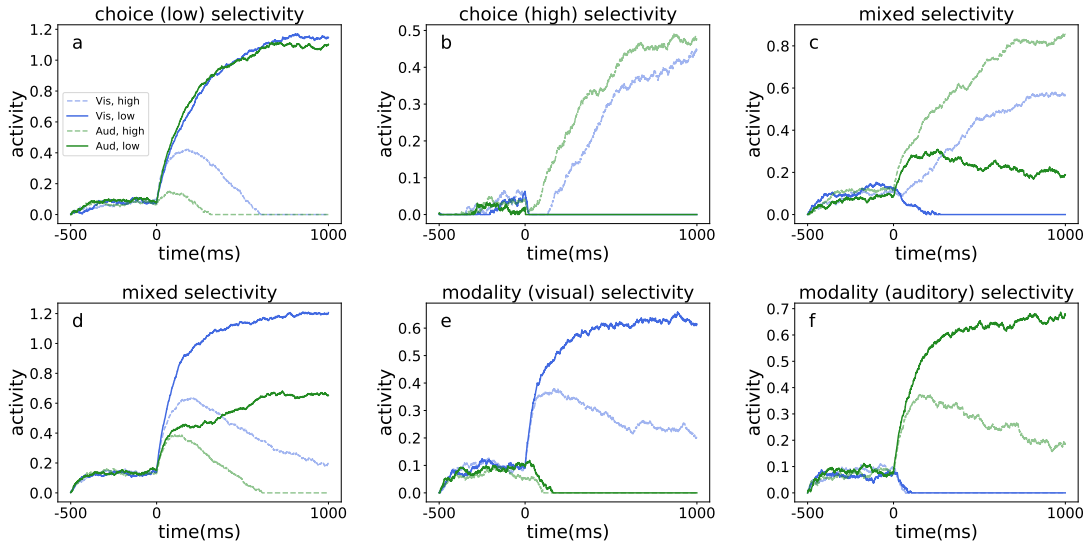


FIG. 15: Selectivity of constituent neurons for the MSI task. Training conditions are the same as in Fig. 10. The neurons show selectivity with respect to choice (a, b), modality (e, f) or both (c, d).



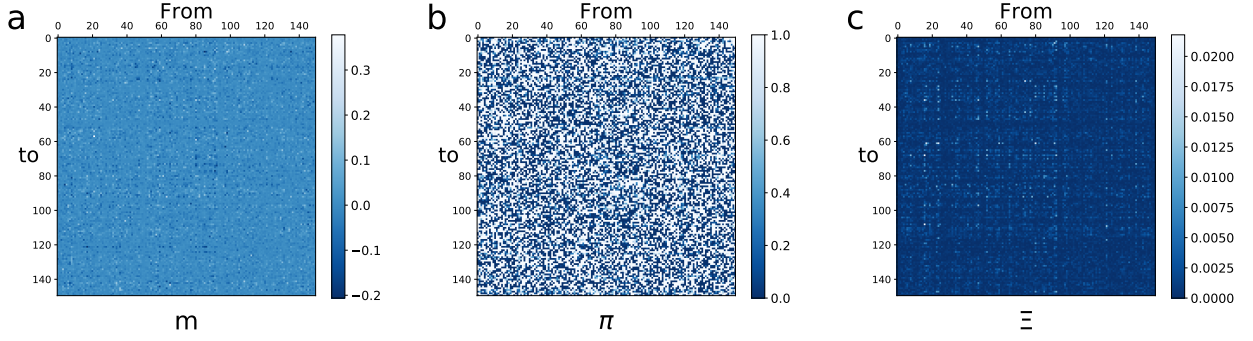


FIG. 16: Hyper-parameter matrix of the recurrent layer in a trained network for the MSI task. Trained conditions are the same as in Fig. 10. Hyper-parameters  $(\pi, m, \Xi)$  are plotted in the matrix form with the dimension  $N \times N$ , where  $N$  indicates the number of neurons in the reservoir.

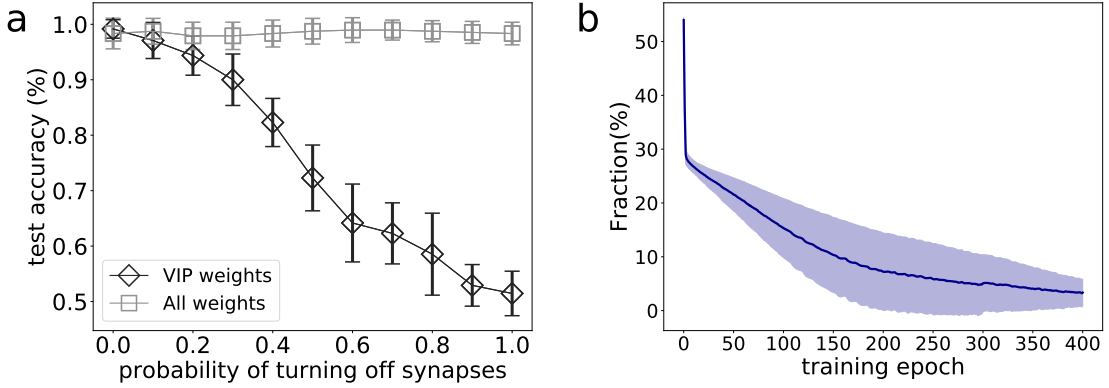


FIG. 17: Targeted-weight perturbation in the recurrent layer for the MSI task. (a) VIP weights (a relaxed version, i.e.,  $\pi < 0.1$ ,  $|m| > 0.05$ , note that  $\Xi$  is very small) are stochastically turned off, in comparison with randomly selected weights pruned with the same number. (b) The fraction of VIP weights changes during the training process. Trained conditions are the same as in Fig. 10.

dynamic network in adaptation of external stimuli could shed light on our understanding of adaptive RNNs.

#### IV. CONCLUSION

In this study, we propose an ensemble perspective for understanding temporal credit assignment, which yields a generalized BPTT algorithm for training RNNs in practice. Our training protocol produces the hyperparameters underlying the weight distribution, or the statistics of the RNN ensemble. In contrast to the standard BPTT, gBPTT highlights the importance of network statistics, which can particularly make a dynamic network changing its specified network weights a potential substrate for recurrent computation in adaptation to sensory inputs. It is thus interesting in future works to explore the biological counterpart of neural computation in brain circuits, e.g., in terms of dendritic spine dynamics [25].

Our SaS model has three types of hyperparameters with distinct roles.  $m$  tells us the mean of the continuous Gaussian slab, while  $\Xi$  controls the variance (fluctuation) of the slab. In both computational tasks we are interested in, we find that the  $\Xi$ -distribution profile is L-shaped. In other words, the peak at zero turns the SaS distribution into a Bernoulli distribution, while the tail at finite values of variance endows a computational flexibility to each connection, which may be critical to recode the high-dimensional sensory inputs into a low-dimensional latent dynamics. It is thus interesting to establish this hypothesis, by addressing precisely how the ensemble perspective helps to clarify the mechanism of low-dimensional latent dynamics encoding relevant spatio-temporal features of inputs.

The spike probability  $\pi$  tells us the sparsity level of the network. We find that a sparse RNN emerges after training. In particular, the recurrent layer is sparser than the output layer, reflecting different roles of both layers. The sparseness allows the recurrent layer to remove some unnecessary degrees of freedom in the recurrent dynamics, making recurrent feedbacks maintain only relevant information for decision making. In contrast, the output layer is

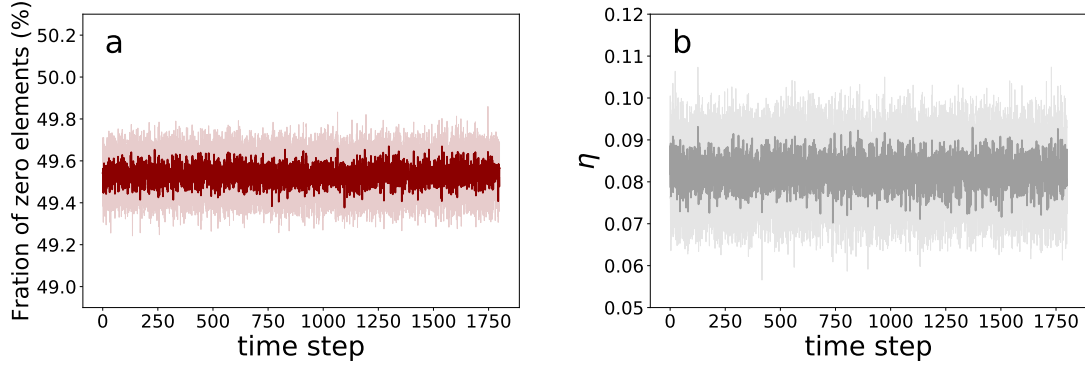


FIG. 18: The statistics of the dynamic network implementing the MSI task could be preserved. (a) The fraction of zero elements of sampled weights across one test trial. The fluctuation is computed from ten independent runs. (b) The asymmetry measure  $\eta$  defined by  $\frac{\overline{w_{ij}w_{ji}}}{w_{ij}^2}$  versus time step. The over-bar means the average over all reciprocal connections. The result is averaged over ten independent runs.

much denser, being thus able to read out relevant information both completely and robustly (note that most of  $\Xi$  values are zero). It is worth noticing that the  $\pi$ -distribution profile implies the existence of VIP weights, which we show has a critical contribution to the overall performance of the network. Our method thus provides a practical way to identify the critical elements of the network topology, which could contribute to understanding temporal credit assignment underlying the behavior of the RNN.

Working at the ensemble level, the constituent neurons of our model also display neural selectivity of different nature in response to the task parameters. Some neurons show uni-selectivity, while the others show mixed selectivity. The selectivity property of neurons, shaped by the recurrent connections, is also a key factor impacting the behavioral output of the network, and thus deserves future studies about the structure basis of the neural selectivity.

Taken together, our model and the associated training method are able to provide insights toward a precise understanding of temporal credit assignment, not only in engineering applications (e.g., MNIST digit classification), but also in modeling brain dynamics (e.g., multisensory integration task).

### Acknowledgments

This research was supported by the National Natural Science Foundation of China for Grant No. 11805284 and the start-up budget 74130-18831109 of the 100-talent-program of Sun Yat-sen University.

- 
- [1] Sepp Hochreiter and Jurgen Schmidhuber. Long short-term memory. *Neural Computation*, 9(8):1735–1780, 1997.
  - [2] Alex Graves. Generating sequences with recurrent neural networks. *arXiv:1308.0850*, 2013.
  - [3] Ilya Sutskever, Oriol Vinyals, and Quoc V. Le. Sequence to sequence learning with neural networks. In *Advances in Neural Information Processing Systems 27*, pages 3104–3112, 2014.
  - [4] Dzmitry Bahdanau, Kyunghyun Cho, and Yoshua Bengio. Neural machine translation by jointly learning to align and translate. In *ICLR 2015 : International Conference on Learning Representations 2015*, 2015.
  - [5] Kyunghyun Cho, Bart van Merriënboer, Caglar Gulcehre, Dzmitry Bahdanau, Fethi Bougares, Holger Schwenk, and Yoshua Bengio. Learning phrase representations using rnn encoder-decoder for statistical machine translation. *arXiv:1406.1078*, 2014.
  - [6] Junyoung Chung, Caglar Gulcehre, KyungHyun Cho, and Yoshua Bengio. Empirical evaluation of gated recurrent neural networks on sequence modeling. *arXiv:1412.3555*, 2014.
  - [7] Saurabh Vyas, Matthew D. Golub, David Sussillo, and Krishna V. Shenoy. Computation through neural population dynamics. *Annual Review of Neuroscience*, 43(1):249–275, 2020.
  - [8] James M Murray. Local online learning in recurrent networks with random feedback. *eLife*, 8:e43299, 2019.
  - [9] Dean V. Buonomano and Wolfgang Maass. State-dependent computations: spatiotemporal processing in cortical networks. *Nature Reviews Neuroscience*, 10(2):113–125, 2009.
  - [10] Thomas Miconi. Biologically plausible learning in recurrent neural networks reproduces neural dynamics observed during cognitive tasks. *eLife*, 6:e20899, 2017.



- [11] Jeffrey L. Elman. Finding structure in time. *Cognitive Science*, 14(2):179–211, 1990.
- [12] P. J. Werbos. Backpropagation through time: what it does and how to do it. *Proceedings of the IEEE*, 78(10):1550–1560, 1990.
- [13] Chan Li and Haiping Huang. Learning credit assignment. *Phys. Rev. Lett.*, 125:178301, 2020.
- [14] Alexandre Pouget, Jeffrey M Beck, Wei Ji Ma, and Peter E Latham. Probabilistic brains: knowns and unknowns. *Nature Neuroscience*, 16(9):1170–1178, 2013.
- [15] Quoc V. Le, Navdeep Jaitly, and Geoffrey E. Hinton. A simple way to initialize recurrent networks of rectified linear units. *arXiv:1504.00941*, 2015.
- [16] Ladan Shams and Aaron R. Seitz. Benefits of multisensory learning. *Trends in Cognitive Sciences*, 12(11):411–417, 2008.
- [17] Dora E Angelaki, Yong Gu, and Gregory C DeAngelis. Multisensory integration: psychophysics, neurophysiology, and computation. *Current Opinion in Neurobiology*, 19(4):452–458, 2009.
- [18] Chandramouli Chandrasekaran. Computational principles and models of multisensory integration. *Current Opinion in Neurobiology*, 43:25–34, 2017.
- [19] Yuhuang Hu, Adrian E. G. Huber, Jithendar Anumula, and Shih-Chii Liu. Overcoming the vanishing gradient problem in plain recurrent networks. *arXiv:1801.06105*, 2018.
- [20] Daniel T. Gillespie. Exact numerical simulation of the ornstein-uhlenbeck process and its integral. *Physical Review E*, 54(2):2084–2091, 1996.
- [21] H. Francis Song, Guangyu R. Yang, and Xiao-Jing Wang. Training excitatory-inhibitory recurrent neural networks for cognitive tasks: A simple and flexible framework. *PLOS Computational Biology*, 12:e1004792, 2016.
- [22] David Raposo, John P. Sheppard, Paul R. Schrater, and Anne K. Churchland. Multisensory decision-making in rats and humans. *The Journal of Neuroscience*, 32(11):3726–3735, 2012.
- [23] Cengiz Pehlevan and Haim Sompolinsky. Selectivity and sparseness in randomly connected balanced networks. *PLOS ONE*, 9(2):e89992, 2014.
- [24] Mattia Rigotti, Omri Barak, Melissa R. Warden, Xiao Jing Wang, Nathaniel D. Daw, Earl K. Miller, and Stefano Fusi. The importance of mixed selectivity in complex cognitive tasks. *Nature*, 497(7451):585–590, 2013.
- [25] Nobuaki Yasumatsu, Masanori Matsuzaki, Takashi Miyazaki, Jun Noguchi, and Haruo Kasai. Principles of long-term dynamics of dendritic spines. *The Journal of Neuroscience*, 28(50):13592–13608, 2008.
- [26] D. Harshad Bhatt, Shengxiang Zhang, and Wen-Biao Gan. Dendritic spine dynamics. *Annual Review of Physiology*, 71(1):261–282, 2009.
- [27] Seungdae Baek, Min Song, Jaeson Jang, Gwangsu Kim, and Se-Bum Paik. Spontaneous generation of face recognition in untrained deep neural networks. *bioRxiv*, 2019.
- [28] David Raposo, Matthew T Kaufman, and Anne K Churchland. A category-free neural population supports evolving demands during decision-making. *Nature Neuroscience*, 17(12):1784–1792, 2014.
- [29] Paul Miller, Carlos D. Brody, Ranulfo Romo, and Xiao Jing Wang. A recurrent network model of somatosensory parametric working memory in the prefrontal cortex. *Cerebral Cortex*, 13(11):1208–1218, 2003.